Interface-Governed Deformation of Nanobubbles and Nanotents Formed by Two-Dimensional Materials

Zhaohe Dai, Yuan Hou, Daniel A. Sanchez, Guorui Wang, Christopher J. Brennan, Zhong Zhang, Luqi Liu, and Nanshu Lu

1   **Interface-Governed Deformation of Nanobubbles and Nanotents formed by Two-**

2   **Dimensional Materials**

3   Zhaohe Dai [1], Yuan Hou [2], Daniel A. Sanchez [3], Guorui Wang [2], Christopher J. Brennan [4], Zhong

4   Zhang [2], Luqi Liu [2], Nanshu Lu [1, 3, 4, 5]

5   [1] *Center for Mechanics of Solids, Structures and Materials, Department of Aerospace*

6   *Engineering and Engineering Mechanics, The University of Texas at Austin, Austin, Texas 78712,*

7   *USA.*

8   [2] *CAS Key Laboratory of Nanosystem and Hierarchical Fabrication, CAS Center for Excellence*

9   *in Nanoscience National Center for Nanoscience and Technology, Beijing 100190, China.*

10   [3] *Texas Materials Institute, The University of Texas at Austin, Austin, Texas 78712, USA.*

11   [4] *Department of Electrical and Computer Engineering, The University of Texas at Austin, Austin,*

12   *Texas, 78712, USA.*

13   [5] *Department of Biomedical Engineering, The University of Texas at Austin, Austin, Texas,*

14   *78712, USA.*

15   Correspondence and requests for materials should be addressed to Nanshu Lu (email:

16   nanshulu@utexas.edu) or Luqi Liu (email: liulq@nanoctr.cn).

17

18   **Abstract**

19   Nanoblisters such as nanobubbles and nanotents formed by two-dimensional (2D) materials have been

20   extensively exploited for strain engineering purposes as they can produce self-sustained, non-uniform in-

21   plane strains through out-of-plane deformation. However, deterministic measure and control of strain

22   fields in these systems are challenging because of the atomic thinness and unconventional interface

23   behaviors of 2D materials. Here, we experimentally characterize a simple and unified power law for the

24   profiles of a variety of nanobubbles and nanotents formed by 2D materials such as graphene and MoS_2

25   layers. Using membrane theory, we analytically unveil what sets the in-plane strains of these blisters

26   regarding their shape and interface characteristics. Our analytical solutions are validated by Raman

27   spectroscopy measured strain distributions in bulged graphene bubbles supported by strong and weak

28   shear interfaces. We advocate that both the strain magnitudes and distributions can be tuned by the 2D

29   material-substrate interface adhesion and friction properties.

30

31   **Keywords**: 2D materials; strain engineering; out-of-plane deformation; interface; membrane theory

32   Two-dimensional (2D) materials are atomically thin crystals with unique properties that lend well to

33   next-generation ultrathin electronic and optoelectronic devices [1-4]. It has been well established that

34   mechanical strain can strongly perturb the band structure of these materials, giving rise to the possibility

35   of using mechanical deformation to tune their electronic and photonic performance dramatically [5-9]. In

36   fact, this principle, termed strain engineering, is now routinely used in manufacturing traditional

37   semiconductor devices [10]. The strain engineering of 2D materials is particularly exciting because an

38   individual atomic sheet is intrinsically capable of sustaining much larger mechanical strain compared to

39   either their bulk counterparts or conventional electronic materials [11,12]. Also, the atomic thickness of

40   2D materials allows them to be easily poked or pressurized from the third dimension (i.e. perpendicular to

41   their plane of atoms) [13-17]. The resulting configurations including nanoscale bubbles and tents can be

42   called by a unified name, 2D material blisters [13-20]. Recently, the considerable strain associated with

43   these nanoblisters have created opportunities for the study of new fundamental physics and applications

44   such as enormous pseudo-magnetic fields, large-scale quantum emitters, and so on [21-23].

45   A major challenge in these systems is to find out or even control the strain in the blisters

46   deterministically, calling for understanding and validating how the blister geometry intertwines with

47   mechanics in these atomic sheets [24,25]. So far, self-similar profiles of the 2D material bubbles have

48   been widely discovered in experiments [15,17,26,27]. However, it remains challenging to analytically

49   relate the bubble and tent shape characteristics to the full-field strain distributions and experimentally

50   prove the relation. Consequently, accurate strain tuning through blister shape adjustments is still elusive

51   [21,22,24]. One difficulty comes from the intrinsically nonlinear coupling between in-plane strain and

52   out-of-plane deformations predicted by the membrane theory [28]. More fundamental concern arises from

53   the subtle nature of 2D materials, where the material thickness approaches the atomic scale and the

54   surface is atomically smooth [29]. These features even challenge the applicability of continuum theories

55   from a perspective of deformation physics [30-34]. As a result, the prevailing analysis of the strain

56   distribution and strain-coupled physics and chemistry in 2D material blisters relies heavily on numerical

57   techniques, such as case-by-case molecular dynamics (MD) simulations [22,24,35-37]. To deal with these

58   concerns, a combination of continuum theories with microscale experiments is highly needed and yet to

59   emerge so far.

60   Herein, we experimentally explore the strain field in nanoblisters formed by 2D materials accounting

61   for different natures of 2D materials interfaces. Using tapping mode atomic force microscopy (AFM), we

62   experimentally characterized a variety of bubbles and tents formed by graphene and MoS_2 layers. Their

63   shapes were empirically found to follow a simple power law, enabling closed-form analytical solutions to

64   the Föppl–von Kármán equations at the membrane limit. Our results show that the strain distribution in

65   the 2D material can be estimated by simply measuring the height and radius of the bubbles and tents, and

66   that the strain highly depends on the interfacial interaction between the 2D material and the underlying

67   substrate. To validate our analytical solutions, we experimentally carried out Raman mapping on

68   pressurized graphene nanobubbles with strong (graphene-SiO_2) and weak (graphene-graphene) shear

69   interfaces. The measured and analytically predicted Raman shifts have found good match for both types

70   of interfaces.

71   We first investigate the shape characteristics of both nanobubbles and nanotents of 2D materials,

72   which can form spontaneously or be created in a controllable manner. For the spontaneous case,

73   nanometer-scale bubbles and tents form when monolayer or few-layer 2D materials are exfoliated or

74   transferred on a target substrate. The formation mechanism is typically attributed to the inevitably trapped

75   water, hydrocarbon, and/or nanoparticles at the 2D material-substrate interface during sample preparation

76   [15,17]. The spontaneously formed nanobubbles and nanotents analyzed in this study were made by

77   mechanically exfoliating few- and monolayer graphene and MoS_2 from their bulk crystals on silicon

78   substrate, or transferring CVD-grown MoS_2 on gold or Al_2O_3 substrate [38]. Details on the transfer

79   process for different types of samples are provided in the Methods section [39]. Figure 1a displays typical

80   examples of nanobubbles formed by monolayer graphene on SiO_2. When nanoparticles were trapped, 2D

81   materials can drape around the nanoparticle, forming micro- or nano-tents as shown in Figs. 1b and 1c. To

82   form controllable bubbles, we transferred monolayer graphene and a 4-layer MoS_2 to cover pre-patterned

83   micro-cavities in SiO_2 to form suspended drumheads and then followed a well-established gas diffusion

4

84 procedure to bulge the drumheads [16]. In this case, the bubbles can be pressurized in a controllable

85 manner (Fig. 1d [39]).

86   The out-of-plane profiles of all the different types of bubbles and tents prepared by ourselves and

87 collected from the literature are summarized in Fig. 2. Although the radii of the 2D material blisters range

88 from tens to thousands of nanometers, we realized that the height profiles of bubbles and tents collapse

89 onto two master curves if we normalize the out-of-plane deflection (w) of each blister by its central height

90 (h), and the radial positions (r) by its radius (a). We discovered that the collapsed height profiles can be

91 described by a unified power form,

$$\frac{w}{h} = 1 - \left(\frac{r}{a}\right)^{\alpha} \tag{1},$$

93 where α is 2 for bubbles or 2/3 for tents. Note that Fig. 2 summarizes graphene and MoS_2 bubbles and

94 tents with aspect ratios ranging from 0.05 to 0.20. Remarkably, regardless of the aspect ratios, the types of

95 2D material, the supporting substrates (silicon, alumina, or atomically flat 2D material flakes), the content

96 in the bubble (liquid or gas), or the fabrication methods, all bubble profiles can collapse to Eq. (1) with

97 $\alpha = 2$ (Fig. 2a). We also found that for profiles of graphene and MoS_2 tents, data obtained from MD

98 simulations or coarse-grained (CG) modeling [22,24,36] can also collapse to Eq. (1) with $\alpha = 2/3$ (Fig.

99 2b). In fact, the empirical conclusion of $\alpha = 2$ is a widely adopted simple membrane solution for blisters

100 [48,49] and $\alpha = 2/3$ is well matched with the analytical solution to an indented blister in the literature

101 [28,50]. We thus conclude that this simple power form can be a good approximation for describing the

102 profiles of 2D material bubbles and tents.

103   Now that the out-of-plane displacement of 2D material blisters is readily available as given in Eq. (1),

104 we can try to solve the in-plane displacement and then calculate strains out of displacements. Attributing

105 to the atomic thinness of 2D materials, it is sufficient to simply use the membrane limit of the Föppl–von

106 Kármán equations [28,48]. The in-plane equilibrium equation in terms of displacements is therefore:

$$\frac{d^2u}{dr^2} + \frac{1}{r}\frac{du}{dr} - \frac{u}{r^2} = -\frac{1-v}{2r}\left(\frac{dw}{dr}\right)^2 - \frac{dw}{dr}\frac{d^2w}{dr^2} \tag{2},$$

108   where u is the in-plane displacement of the 2D material and v is the Poisson's ratio. Plugging Eq. (1) into

109   this equation and solving the 2nd order ODE using the finite condition when $r \to 0$ can yield an analytical

110   solution to the in-plane displacement:

111
$$u = \zeta(v)\frac{h^2}{a}\left(\frac{r}{a} - \left(\frac{r}{a}\right)^{2\alpha-1}\right) + u_s\frac{r}{a} \tag{3},$$

112   where $\zeta(v) = \frac{\alpha(2\alpha-1-v)}{8(\alpha-1)}$ and u_s is a constant related to the slippage at the edge of the blister ($r = a$). This

113   explicit displacement field allows for the direct solutions for both the radial and circumferential strain

114   fields:

115
$$\varepsilon_r = \begin{cases} \zeta(v)\frac{h^2}{a^2}\left(1 - \frac{1+v-2\alpha v}{2\alpha-1-v}\left(\frac{r}{a}\right)^{2\alpha-2}\right) + \frac{u_s}{a}, & r \le a \\ -\frac{au_s}{r^2}, & r > a \end{cases} \tag{4a},$$

116
$$\varepsilon_\theta = \begin{cases} \zeta(v)\frac{h^2}{a^2}\left(1 - \left(\frac{r}{a}\right)^{2\alpha-2}\right) + \frac{u_s}{a}, & r \le a \\ \frac{au_s}{r^2}, & r > a \end{cases} \tag{4b}.$$

117   Clearly, the sliding of the 2D material-substrate interface ($u_s \ne 0$) can induce non-zero strain in the

118   supported zone ($r > a$), which is important for strain engineering applications of 2D materials [35].

119   Typically, the edge of the 2D material blister is assumed to be fully clamped due to adhesion and strong

120   shear interactions with the supporting substrate outside of boundary [11,22.16]. However, the atomically

121   smooth surfaces of 2D materials make interfacial sliding particularly easy. Recent experiments on gas-

122   pressurized graphene bubbles revealed that the shear interactions between graphene and its substrate can

123   be fairly weak, leading to nonlinear, deflection-dependent interface sliding displacements [14,51]. It has

124   also been discovered that well-established theories assuming clamped conditions offer good

125   approximations only when the deflection is small ($h/a < 0.1$), while experimental measurements

126   deviated from theories with clamped boundaries in samples with large deflection [14]. Recent studies on

127   2D material interface further highlighted the so-called superlubrication (near-zero friction) when a 2D

128   material sits on atomically smooth substrates, including itself, which is very common in 2D materials

129   devices [52].

130   Considering that the graphene and MoS$_2$ blisters in Fig. 2 encompass either relatively strong

131   interfaces with small deflections or atomically lubricated interfaces, our prime interest of this study is in

132 two limits: strong-shear limit (clamped, fully bonded interface) and weak-shear limit (sliding, frictionless

133 interface). For the former, we can apply clamped boundary at the edge of the blister. For the latter, the

134 stress and displacement in the outer supported region can be obtained as the classical Lamé problem in

135 linear elasticity [53]. The stress and displacement continuity then leads to [39]

136
$$u_s = \begin{cases} 0, & \text{strong} - \text{shear limit} \\ -\frac{\alpha(1+v)}{8}\frac{h^2}{a}, & \text{weak} - \text{shear limit} \end{cases} \tag{5.}$$

137 Now Eq. (4) and Eq. (5) combined offer the complete analytical solutions to the strain field in 2D

138 materials forming blisters, with either strong or weak interaction with their substrates. After appropriately

139 choosing the α and u_s according to the specific blister shape and 2D material-substrate interface, one can

140 easily compute the strain distribution inside and outside of a 2D blister by simply measuring its height

141 and radius. We note that a generalized analysis may be performed by accounting for the detailed frictional

142 resistance (e.g. the stick-slip behavior) at the 2D material-substrate interface [54].

143 In Fig. 3, we plot the strain distributions of the 2D material blister as solid curves using our equations.

144 The strain is normalized by h^2/a^2 such that the distribution will only depend on the interface conditions

145 and material properties, i.e. the Poisson's ratio. Comparing Fig. 3a for bubbles and Fig. 3b for tents, it is

146 clear that the strain gradients are much larger in tents, with strain divergence towards the center of the

147 tents due to the assumed point load. Note that under the same aspect ratio, interface sliding can

148 considerably reduce the strain level in 2D material blisters in comparison with blisters with strong-shear

149 interfaces. This highlights the importance of accounting for the ultra-lubricated interface in the case that

150 the 2D material is supported by an atomically smooth substrate.

151 Next, we try to verify our analytical solutions numerically. We solved the nonlinear Föppl–von

152 Kármán equations with clamped and slipping boundaries, where the bending behavior is also considered

153 for generality [39]. The numerical solutions are plotted as markers in Fig. 3 for monolayer graphene with

154 aspect ratios ranging from 0.05 to 0.20, to directly compare with the analytical solutions (solid curves).

155 Since analytically solved strains are strictly proportional to h^2/a^2, after normalization, the solid curves

156 are no longer dependent on the aspect ratio. However, the numerically solved strains show more

157   complicated dependence on the aspect ratio, because the markers for different aspect ratios do not fully

158   collapse. Despite this small discrepancy, the overall good agreement between the two solutions indicates

159   that for our experimentally observed blisters with aspect ratios ranging from 0.05 to 0.20, bending effects

160   are negligible. Thus, the numerical results have verified that our analytical solution given by Eq. (4) is a

161   reasonable estimation for strains in both bubbles and tents under both clamped and slipping boundary

162   conditions.

163   Our analytical solution, though verified numerically, is still challenged by a widespread concern on

164   the breakdown of classical membrane theories at the atomic limit [30-34]. To examine the applicability of

165   our analytical solutions, we performed graphene bulging experiments with intentionally designed strong-

166   and   weak-shear   interfaces.   Monolayer   graphene   sealed   micro-cavities   were   fabricated   by

167   micromechanical cleavage of graphene over SiO_2 substrate with pre-patterned 2.5-micron-radius holes

168   (Fig. 4a). Following a well-developed gas diffusion method [16], we can create a pressure difference

169   across the monolayer and bulge it in a controlled manner.

170   The strong-shear-interface graphene bubble was generated by pressurizing a graphene monolayer on

171   SiO_2 with the maximum deflection less than 150 nm. Under this condition, the interface sliding was found

172   to be minimal, thus is compatible with the clamped interface assumption [14]. To experimentally study

173   the weak-shear case, we assembled a graphene-SiO_2 supporting substrate for the graphene bubble (Fig.

174   4b). First, few-layer graphene was transferred over a SiO_2 micro-hole. The suspended portion of the

175   multilayer graphene was then etched to open up the micro-hole. After creating an atomically flat region

176   around the micro-hole, a monolayer graphene was precisely transferred to cover this micro-hole, resulting

177   in a graphene drumhead supported by few-layer graphene [39]. Applying a differential pressure across the

178   suspended graphene membrane, this graphene bubble was expected to bulge under weak-shear interface

179   as the graphene-graphene interface can be considered as superlubricated.

180   We performed multiple AFM and Raman characterizations on the graphene bubbles with well-

181   controlled interfaces [39]. For an axisymmetric graphene bubble, the G band shifts in the Raman

182   spectrum are related to the strain components through the following equation [55]:

183
$$\frac{\Delta\omega_G}{\omega_0} = -\gamma(\varepsilon_r + \varepsilon_\theta) \pm \frac{\beta}{2}(\varepsilon_r - \varepsilon_\theta) \tag{6},$$

184 where ε_r and ε_θ are analytically expressed in Eq. (4), γ is the Grüneisen parameter, and β is the shear

185 deformation potential that details the amount of splitting in the G bands, which were experimentally

186 calibrated for monolayer graphene ($\gamma = 1.99$ and $\beta = 0.99$) [56]. Therefore, analytical prediction for

187 strain fields can be readily converted to analytical prediction for the G band shifts using Eq. (6).

188 Particularly, at the center of the bubble where $\varepsilon_r = \varepsilon_\theta$, the G band shifts are predicted by Eq. (4) and Eq.

189 (6) to take a very simple form:

190
$$\Delta\omega_G = -c\gamma\omega_0 \frac{h^2}{a^2} \tag{7}$$

191 where the constant c is $\frac{3-\nu}{2}$ for bubbles supported by strong shear interfaces and is $(1 - \nu)$ by weak shear

192 interfaces.

193   Due to space limitations, we present the details of the experimental Raman characterizations in

194 Supplemental Materials Note 2 [39]. Here, we first show the Raman G band shifts at the center of

195 graphene bubbles as a function of h^2/a^2 in Fig. 4c, which is predicted to be linear by our analytical

196 solution in Eq. (7). The markers represent experimental data for both SiO_2- (brown) and graphene-

197 supported (green) graphene bubbles and the solid curves correspond to predicted G band shifts for strong-

198 (green) and weak-shear-interfaced (brown) 2D material bubbles. By setting the Poisson's ratio of

199 graphene to be 0.165 in Eq. (7), we find good agreement between our theoretical predictions and

200 experimental measurements. This may confirm the applicability of our simplified membrane theory in

201 relating the out-of-plane deformations to in-plane strains for 2D material blisters.

202   In Fig. 4d, we further normalize both the measured and predicted G band shifts by h^2/a^2 and plot

203 them as functions of the normalized radial position r/a. Our weak-shear and strong-shear model can

204 partially capture the full-field strain distribution in graphene-on-graphene and graphene-on-SiO_2 bubbles,

205 respectively. However, deviation between predicted and measured G band shifts occurs and enlarges

206 towards the edge of the bubble, especially for SiO_2-supported graphene bubbles. We attribute such edge

207 deviation in Fig. 4d to the limited spatial resolution of Raman spectroscopy (~1 μm) and the possible

208 doping effect by the substrate [57,58], which are further elucidated in Fig. S9 and S10 [39]. As for 2D

209   material tents, a recent study reported the Raman 2D band shifts for a SiN/Si-supported graphene

210   drumhead subjected to nanoindentation [59]. The experimental results can be well captured by our

211   analytical solution to 2D material tent with strong-shear interface (Fig. S11 [39]). We thus claim that our

212   analytical solutions in Eq. (5), enabled by the shape characteristics in Fig. 2, can offer valid estimation for

213   the in-plane strain in 2D material bubbles and tents simply by knowing their height and radius. It is

214   especially true at the center of bubbles by Eq. (7), which may, in turn, be used to measure the Gru neisen

215   parameter for the broadly extended 2D material family.

216   The 2D material bubble and tent structures have been exploited in many recent studies [17-22,27,60-

217   64], where people typically use pre-patterned micro-pillars or interface-confined contents to produce a

218   single or an array of 2D material blisters. Our findings show that the strain in blisters highly hinges on

219   their aspect ratio (h/a). We note that a balance between adhesion (which favors large areas of contact)

220   and stretching energy (which diminishes in blisters of large radius) dictates a constant aspect ratio:

221    $$h/a = (\phi \Delta \gamma / E_{2D})^{1/4} \tag{8}$$

222   where $\Delta \gamma$ is energy change per unit area, E_{2D} is the in-plane stiffness of the 2D material, and ϕ is a

223   constant prefactor. Equation (8) implies that the aspect ratio or ultimately the strain of a 2D material

224   bubble or tent is dominated by the ratio of the 2D material-substrate adhesion to the in-plane stiffness of

225   the 2D material. In fact, this interface- and stiffness-dependent out-of-plane deformation characteristic has

226   been observed at a variety of length scales — from graphene to polymer films with thicknesses ranging

227   from 1 nm to 1 mm [50]. Here, we determine ϕ for 2D material bubbles and tents of both strong- and

228   weak-shear interfaces in Table 1 [39]. Notably, recent experimental discovery of the constant aspect ratio

229   of 2D material bubbles for a given 2D material-substrate system provided a good validation [17], and

230   there is no available experimental data for 2D material tents so far.

231

236

Figure Captions

FIG. 1. From top to bottom: atomic force microscopy (AFM) phase and height images of spontaneously formed graphene bubbles on SiO_2 (a), a multilayer graphene tent on SiO_2 (b), and a CVD-MoS_2 tent on gold film (c). (d) From left to right: optical image of graphene flakes exfoliated on pre-patterned SiO_2 with micro-cavities, AFM height images of a monolayer graphene bubble, and a 4-layer MoS_2 bubble. Note that (S) represents bubbles or tents formed spontaneously while (P) represents those formed by controllable air pressurization. The unit for all height bars is nm.

FIG. 2. Universal shape characteristics of 2D material bubbles and tents. (a) Normalized bubble profiles measured by our experiments and collected from literature. Note that samples from Ref. [17] feature atomically smooth interfaces, are labeled by *. (b) Normalized tent profiles measured by our experiments and simulation results in the literature. The simulation data about graphene and MoS_2 is from Ref. [36] and Ref. [24], respectively.

FIG. 3. Normalized strain distribution curves predicted by our analytical solution (solid lines) and solved by numerical analysis (markers) in bubbles (a) and tents (b), subjected to both clamped (strong interface) and frictionless (sliding interfaces) boundary conditions. The strain is normalized by h^2/a^2, giving rise to deflection-independent curves. The numerical results are solved for a monolayer graphene with aspect ratios ranging $0.02 < h/a < 0.2$.

FIG. 4. Schematics of the graphene drumheads formed on a SiO_2 substrate (a) and on a graphene-covered SiO_2 substrate (b). (c) Raman shifts of the G band at the center of graphene bubbles predicted by our analytical solution (solid curves) and measured by our experiments (markers). (d) Normalized Raman shifts of the G band ($\Delta\omega_G a^2/\omega_0 h^2$) as functions of the normalized radial position (r/a) for monolayer graphene bubbles.

Table 1. The prefactor ϕ that determines the aspect ratio by $\Delta\gamma/E_{2D}$ in Eq. (8).			
	Shape	**Strong shear**	**Weak shear**
Bubble		$\dfrac{24(1-\nu)}{5(7-\nu)}$	$\dfrac{6}{5}$
Tent		$\dfrac{72(1-\nu)}{5-3\nu}$	18

270

Figure 1

271
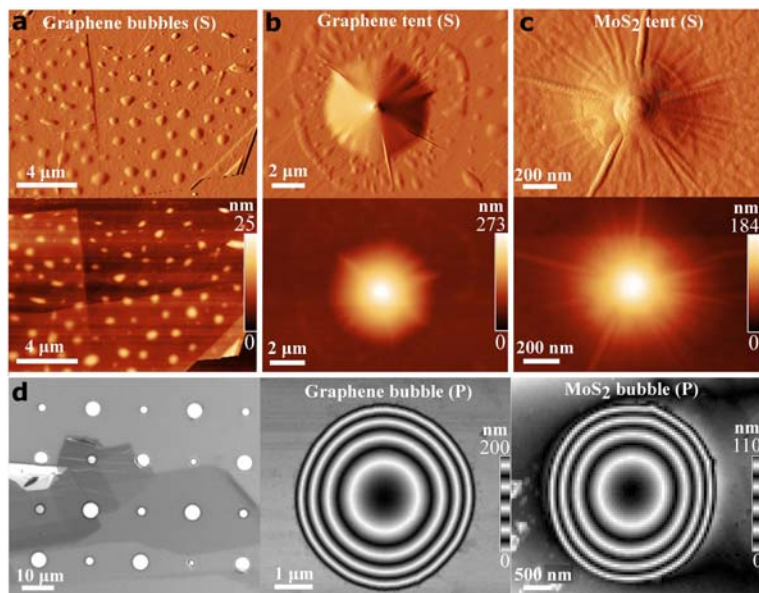
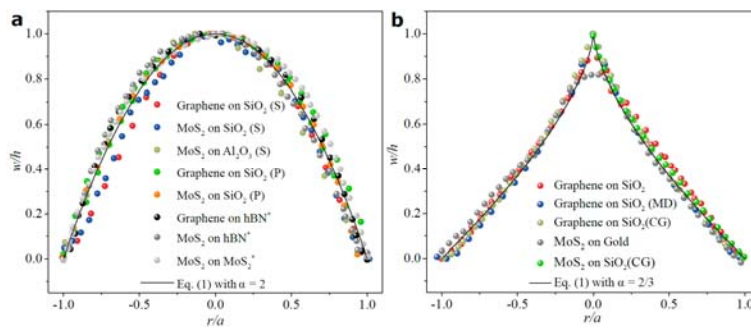272

273

274   **Figure 2**
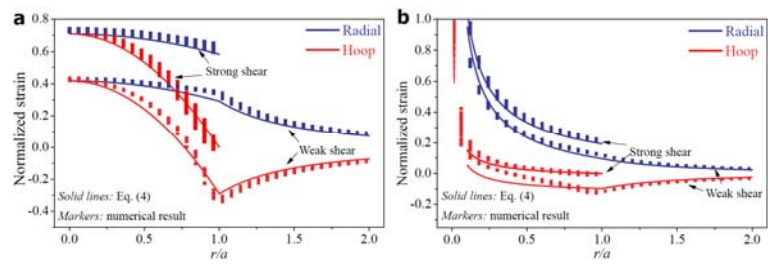

275

276

Figure 3
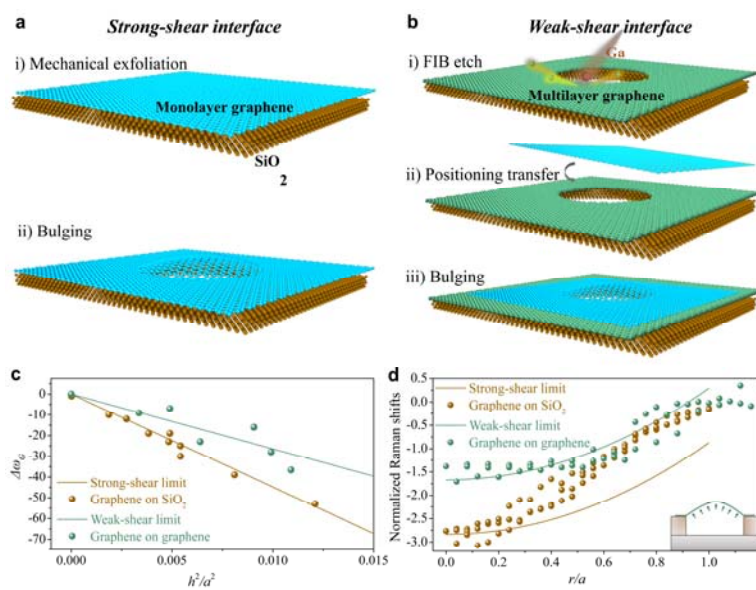
Figure 4

283   [1]   R. Mas-Balleste, C. Gomez-Navarro, J. Gomez-Herrero, and F. Zamora, Nanoscale **3**, 20 (2011).

284   [2]   K. S. Novoselov, A. Mishchenko, A. Carvalho, and A. H. Castro Neto, Science **353** (2016).

285   [3]   D. Akinwande, N. Petrone, and J. Hone, Nat. Commun. **5**, 5678 (2014).

286   [4]   C. Choi *et al.*, Nat. Commun. **8**, 1664 (2017).

287   [5]   D. Lloyd, X. Liu, J. W. Christopher, L. Cantley, A. Wadehra, B. L. Kim, B. B. Goldberg, A. K.
288   Swan, and J. S. Bunch, Nano Lett. **16**, 5836 (2016).

289   [6]   A. Branny, S. Kumar, R. Proux, and B. D. Gerardot, Nat. Commun. **8** (2017).

290   [7]   H. Li *et al.*, Nat. Commun. **6** (2015).

291   [8]   G. G. Naumis, S. Barraza-Lopez, M. Oliva-Leyva, and H. Terrones, Rep. Prog. Phys. **80**, 096501
292   (2017).

293   [9]   G. da Cunha Rodrigues, P. Zelenovskiy, K. Romanyuk, S. Luchkin, Y. Kopelevich, and A.
294   Kholkin, Nat. Commun. **6** (2015).

295   [10] J. A. Del Alamo, Nature **479**, 317 (2011).

296   [11] C. Lee, X. Wei, J. W. Kysar, and J. Hone, Science **321**, 385 (2008).

297   [12] C. Androulidakis, K. Zhang, M. Robertson, and S. H. Tawfick, 2D Mater. **5**, 032005 (2018).

298   [13] D. Davidovikj, F. Alijani, S. Cartamil-Bueno, H. Zant, M. Amabili, and P. Steeneken, Nat.
299   Commun. **8**, 1253 (2017).

300   [14] G. Wang, Z. Dai, Y. Wang, P. Tan, L. Liu, Z. Xu, Y. Wei, R. Huang, and Z. Zhang, Phys. Rev.
301   Lett. **119**, 036101 (2017).

302   [15] D. A. Sanchez, Z. Dai, P. Wang, A. Cantu-Chavez, C. J. Brennan, R. Huang, and N. Lu, Proc.
303   Natl. Acad. Sci. U.S.A. **115**, 7884 (2018).

304   [16] S. P. Koenig, N. G. Boddeti, M. L. Dunn, and J. S. Bunch, Nat. Nanotechnol. **6**, 543 (2011).

305   [17] E. Khestanova, F. Guinea, L. Fumagalli, A. K. Geim, and I. V. Grigorieva, Nat. Commun. **7**,
306   12587 (2016).

307   [18] A. Reserbat-Plantey *et al.*, Nano Lett. **14**, 5044 (2014).

308   [19] H. Tomori, A. Kanda, H. Goto, Y. Ootuka, K. Tsukagoshi, S. Moriyama, E. Watanabe, and D.
309   Tsuya, Appl. Phys. Express **4**, 075102 (2011).

310   [20] J. M. Lee *et al.*, Nano Lett. **10**, 2783 (2010).

311   [21] N. Levy, S. Burke, K. Meaker, M. Panlasigui, A. Zettl, F. Guinea, A. C. Neto, and M. Crommie,
312   Science **329**, 544 (2010).

313   [22] N. N. Klimov, S. Jung, S. Zhu, T. Li, C. A. Wright, S. D. Solares, D. B. Newell, N. B. Zhitenev,
314   and J. A. Stroscio, Science **336**, 1557 (2012).

315   [23] C. Palacios-Berraquero *et al.*, Nat. Commun. **8**, 15093 (2017).

316   [24] J. Feng, X. Qian, C.-W. Huang, and J. Li, Nat. Photonics **6**, 866 (2012).

317   [25] D. Vella and B. Davidovitch, Soft Matter **13**, 2264 (2017).

318   [26] G. Zamborlini *et al.*, Nano Lett. **15**, 6162 (2015).

319   [27] H. Ghorbanfekr-Kalashami, K. S. Vasu, R. R. Nair, F. M. Peeters, and M. Neek-Amal, Nat.
320   Commun. **8**, 15844 (2017).

321   [28] E. H. Mansfield, *The bending and stretching of plates* (Cambridge University Press, 2005).

322   [29] X. Li, L. Tao, Z. Chen, H. Fang, X. Li, X. Wang, J.-B. Xu, and H. Zhu, Appl. Phys. Rev. **4**,
323   021306 (2017).

324   [30] G. López-Polín, C. Gómez-Navarro, V. Parente, F. Guinea, M. I. Katsnelson, F. Pérez-Murano,
325   and J. Gómez-Herrero, Nat. Phys. **11**, 26 (2015).

326   [31] L. Tapasztó, T. Dumitrică, S. J. Kim, P. Nemes-Incze, C. Hwang, and L. P. Biró, Nat. Phys. **8**,
327   739 (2012).

328   [32] J. Los, A. Fasolino, and M. Katsnelson, Phys. Rev. Lett. **116**, 015901 (2016).

329   [33] R. J. Nicholl, N. V. Lavrik, I. Vlassiouk, B. R. Srijanto, and K. I. Bolotin, Phys. Rev. Lett. **118**,
330   266101 (2017).

331   [34] D.-B. Zhang, E. Akatyeva, and T. Dumitrică, Phys. Rev. Lett. **106**, 255503 (2011).

332   [35] Z. Qi, A. L. Kitt, H. S. Park, V. M. Pereira, D. K. Campbell, and A. C. Neto, Phys. Rev. B **90**,
333   125419 (2014).

334	[36]	S. Zhu, Y. Huang, N. N. Klimov, D. B. Newell, N. B. Zhitenev, J. A. Stroscio, S. D. Solares, and
335		T. Li, Phys. Rev. B **90**, 075426 (2014).
336	[37]	Z. Meng, R. A. Soler-Crespo, W. Xia, W. Gao, L. Ruiz, H. D. Espinosa, and S. Keten, Carbon
337		**117**, 476 (2017).
338	[38]	Y. Huang, E. Sutter, N. N. Shi, J. Zheng, T. Yang, D. Englund, H. J. Gao, and P. Sutter, ACS
339		Nano **9**, 10612 (2015).
340	[39]	See Supplementary Material for material preparations, experimental setup and characterizations,
341		and analysis based on membrane mechanics, which includes Refs. [40-47]
342	[40]	C. J. Brennan, R. Ghosh, K. Koul, S. K. Banerjee, N. Lu, and E. T. Yu, Nano Lett. **17**, 5464
343		(2017).
344	[41]	R. Frisenda, E. Navarro-Moratalla, P. Gant, D. Perez De Lara, P. Jarillo-Herrero, R. V.
345		Gorbachev, and A. Castellanos-Gomez, Chem. Soc. Rev. **47**, 53 (2018).
346	[42]	Y. Zhang, C. Hui, R. Sun, K. Li, K. He, X. Ma, and F. Liu, Nanotechnology **25**, 135301 (2014).
347	[43]	L. G. Cancado et al., Nano Lett. **11**, 3190 (2011).
348	[44]	A. C. Ferrari, Solid State Commun. **143**, 47 (2007).
349	[45]	C. Metzger et al, Nano Lett. **10**, 6 (2009).
350	[46]	Z. H. Ni, T. Yu, Y. H. Lu, Y. Y. Wang, Y. P. Feng, and Z. X. Shen, ACS Nano **2**, 2301 (2008).
351	[47]	K. M. Yue, W. Gao, R. Huang, and K. M. Liechti, J. Appl. Phys. **112**, 083512 (2012).
352	[48]	L. B. Freund and S. Suresh, *Thin film materials: stress, defect formation and surface evolution*
353		(Cambridge University Press, 2004).
354	[49]	P. Wang, W. Gao, Z. Cao, K. M. Liechti, and R. Huang, J. Appl. Mech. **80**, 040905 (2013).
355	[50]	J. Chopin, D. Vella, and A. Boudaoud, Proc. R. Soc. A **464**, 2887 (2008).
356	[51]	A. L. Kitt, Z. Qi, S. Rémi, H. S. Park, A. K. Swan, and B. B. Goldberg, Nano Lett. **13**, 2605
357		(2013).
358	[52]	O. Hod, M. Urbakh, D. Naveh, M. Bar Sadan, and A. Ismach, Adv. Mater. 1706581 (2018).
359	[53]	M. H. Sadd, *Elasticity: theory, applications, and numerics* (Academic Press, 2009).
360	[54]	Q. Li, C. Lee, R. W. Carpick, and J. Hone, Phys. Status Solidi B **247**, 2909 (2010).
361	[55]	M. Huang, H. Yan, C. Chen, D. Song, T. F. Heinz, and J. Hone, Proc. Natl. Acad. Sci. U.S.A. **106**,
362		7304 (2009).
363	[56]	T. Mohiuddin *et al.*, Phys. Rev. B **79**, 205433 (2009).
364	[57]	J. E. Lee, G. Ahn, J. Shim, Y. S. Lee, and S. Ryu, Nat. Commun. **3**, 1024 (2012).
365	[58]	A. Das *et al.*, Nat. Nanotechnol. **3**, 210 (2008).
366	[59]	K. Elibol, B. C. Bayer, S. Hummel, J. Kotakoski, G. Argentero, and J. C. Meyer, Sci. Rep. 6,
367		28485 (2016).
368	[60]	K. Xu, P. Cao, and J. R. Heath, Science **329**, 1188 (2010).
369	[61]	K. Vasu *et al.*, Nat. Commun. **7**, 12168 (2016).
370	[62]	Z. Chen *et al.*, Nat. Commun. **8**, 14548 (2017).
371	[63]	Y. Jiang, J. Mao, J. Duan, X. Lai, K. Watanabe, T. Taniguchi, and E. Y. Andrei, Nano Lett. **17**,
372		2839 (2017).
373	[64]	D. Akinwande *et al.*, Extreme Mech. Lett. **13**, 42 (2017).
374		